Journal of Non-Newtonian Fluid Mechanics 222 (2015) 141–150

Contents lists available at ScienceDirect

Journal of Non-Newtonian Fluid Mechanics

journal homepage: http://www.elsevier.com/locate/jnnfm

Modelling the interfacial peeling of pressure-sensitive adhesives ☆

I.K. Mohammed, M.N. Charalambides *, A.J. Kinloch

Department of Mechanical Engineering, Imperial College London, South Kensington, London SW7 2AZ, UK

ARTICLE INFO

Article history:
Received 3 June 2014
Received in revised form 14 October 2014
Accepted 15 October 2014
Available online 8 November 2014

Keywords:
Pressure-sensitive adhesive
Peeling
Finite element
Viscoelastic
Cohesive zones
Tack

ABSTRACT

Peel tests were performed using specimens which consisted of a polyester backing membrane supporting an acrylic pressure-sensitive adhesive adhered to a polyethylene substrate. Interfacial separation of the PSA from the polyethylene substrate was observed. Finite element (FE) peeling simulations were conducted which modelled the backing-membrane as an elasto-plastic power-law material, the adhesive as a viscoelastic material and the interfacial properties with a cohesive zone model (CZM). The material properties of the backing membrane and the pressure-sensitive adhesive were measured from tensile and stress relaxation experiments. The cohesive zone parameters were calculated analytically from the peel test data, as well as being measured directly from independent poker-chip probe tack tests. The numerical results from the CZM/FE simulations and the experimental values of the peel forces as a function of the peel angle were found to be in good agreement.

© 2014 The Authors. Published by Elsevier B.V. This is an open access article under the CC BY license (http://creativecommons.org/licenses/by/3.0/).

1. Introduction

Pressure-sensitive adhesives (PSA) are used in a wide variety of applications such as adhesive tapes [1], product labels, postage stamps [2,3], paper note pads, transdermal patches [4–6] and clothing [7]. Amongst the various classes of adhesives, PSAs are unique because they do not require heat or chemical treatment in order to give a relatively good adhesive strength to a wide range of substrates. For example, unlike structural adhesives, the bond does not need to be formed while the adhesive is in a liquid state. Typical PSA products consist of the PSA material sandwiched between a flexible backing membrane, such as a plastic film, a paper film or a metal foil, and a release liner with a low surface energy.

The PSA surface has to be kept clean of impurities, such as dust, throughout its shelf life or it will lose its adhesion properties, hence the protection of the PSA surface is an important feature with PSAs. For example, PSA labels are adhered to a removable protective sheet known as a release liner while in rolls of PSA tape the top surface of the backing membrane is coated with a low surface energy material to ensure easy removal.

PSAs tend to be elastomeric in nature and the most widely used elastomer is natural rubber, although synthetic rubber-, acrylic- and silicone-based PSAs are common. Rubber based PSAs are the cheapest and simplest to produce, comprising of natural rubber and a tackifying resin. Acrylic PSAs, such as that used in the present study, are typically random copolymers of a long side-chain acrylic polymer (e.g. n-butyl acrylate or 2-ethylhexyl acrylate) with a low glass transition temperature T_g, a short side-chain acrylic such as methyl acrylate to adjust the T_g, and acrylic acid to improve the adhesion. Unlike other types of PSAs, such as those based upon natural rubber, tackifiers are not necessary with acrylic-based PSAs [1] but, to form a good bond to a substrate surface, the PSA must have some degree of tack.

Tack is an important property of a PSA as it quantifies its ability to form instantly a bond when brought into contact with a surface. The final adhesion and cohesive strength of the bond are influenced by numerous factors including the surface energies of the adhesive and substrate, dwell time, contact pressure, mechanical properties of the adhesive, as well as environmental conditions such as temperature and humidity [8]. Therefore, tack is important in many applications where an instant bond is required, however it is equally important when a 'clean' separation of the initially bonded surfaces is desirable. Many different methods for measuring the tack have been devised with the four main ones being the rolling ball, loop tack, quick stick and probe tack tests [9]. Each has its own advantages and disadvantages and the specific testing method should be selected based on the particular application.

The probe tack test is a quantifiable mechanical method of mimicking the subjective thumb/finger test. A flat or spherical probe is brought into contact with the tacky material until a chosen load is reached (known as the dwell force) and then held at that position for a period of time (known as the dwell time). The probe is then pulled away from the specimen at a constant speed until total separation is reached and the load–displacement-time relationship is recorded. The area under the load–displacement curve is referred to as the tack energy, or the tack work of adhesion,

☆ Dedicated to Prof Ken Walters FRS on the occasion of his 80th Birthday.

* Corresponding author. Tel.: +44 (0)20 7594 7246.
E-mail address: m.charalambides@imperial.ac.uk (M.N. Charalambides).

http://dx.doi.org/10.1016/j.jnnfm.2014.10.005
0377-0257/© 2014 The Authors. Published by Elsevier B.V.
This is an open access article under the CC BY license (http://creativecommons.org/licenses/by/3.0/).

W_a, while the peak load can be converted into a maximum stress. Multiple authors have reported tests to determine the effect of parameters such as the dwell time, dwell force, surface roughness, sample aspect ratio and probe material [10–13].

The separation of two surfaces requires an amount of energy dissipation which can be measured using peeling experiments. In such tests the peel force is measured, which may depend on the peeling speed, peel angle, backing membrane thickness and adhesive thickness. Although peel tests are relatively simple to perform [14–16], modelling of the peeling process accurately is a challenge [17]. Finite element (FE) simulations require as an input the material properties of the backing membrane and the adhesive, as well as a damage criterion to represent failure of the adhesive or debonding of the interface, whichever is the observed mode of fracture.

Common techniques for modelling the peel test include the cohesive zone model (CZM) [17,18], virtual crack closure [19], xfem [20] or a critical stress at a distance [21] failure criterion. Numerous authors have modelled the peel test but the majority of these have focused on peel tests which consist of relatively thick metallic peel arms bonded using high modulus structural adhesives. For example, Diehl [22] attempted to create an Abaqus benchmark for the modelling of peeling using a CZM in which the value of the fracture energy was fixed. An aluminium peel arm, modelled using a plastic power-law expression, and an epoxy adhesive, modelled as a simple linear-elastic material, were implemented into the CZM/FE simulation. The cohesive failure of the epoxy was modelled using a layer of zero-thickness cohesive elements with a triangular traction-separation law. The fracture energy was kept constant while the critical stress and failure separation, and hence the initial stiffness, were varied over two orders of magnitude. The peel force that was numerically predicted was in good agreement with the experimentally measured value of the peel force; this demonstrated that the predicted peel force was independent of the value of the critical stress employed in the traction-separation law implemented in the CZM.

Cui et al. [23] used a critical von Mises effective strain at the crack tip as a failure criterion. Aluminium peel arms of different thicknesses were modelled with an epoxy adhesive which exhibited cohesive failure during the peel test. The model was calibrated based on the experimental data of the 90° peel tests until the numerical and experimental peel force values were in agreement. The critical strain was found to be a function of the peel arm thickness but independent of the peel angle.

Martiny et al. [24] developed a quasi-static steady-state FE model of the wedge-peel and fixed arm peel tests. In their model, the local fracture process ahead of the crack front was accounted for by embedding a cohesive zone between layers of elastic–plastic solid elements which represented the adhesive and the substrates. The substrate material was aluminium alloy and the adhesive was an epoxy-based paste adhesive. They validated their model by comparing their predictions with the experimentally measured peel force and radius of curvature for three different peel angles, as well as the fracture energy obtained from independent linear-elastic fracture mechanics tests. Good agreement between the modelling and experimental studies was recorded.

Wei and Hutchinson [25] developed a steady-state peeling model of a rate-independent elastic–plastic film bonded to a substrate in which the interface (i.e. adhesive) thickness was taken to be zero. A CZM was used with the two important parameters being the peak stress and the work of fracture, since the specific shape of the traction-separation law was determined to be unimportant. They also showed that for peel angles less than 90°, the test was predominantly Mode I. Their model was limited to peak stress/yield stress ratios of less than six where the yield stress used was that of the peel arm.

Williams and Kauzlarich [26,27] have performed fixed arm and mandrel peeling experiments with both acrylic and silicone PSAs, and subsequently modelled their tests using the FE software CAE-FEM90. They modelled the PSA layer using an elastic–plastic material model with an adjusted modulus to account for the constraint introduced in a thin film. The strain energy density was measured from the FE output and summed over the peel front in order to predict the value of the 'de-adhesion energy', which was in good agreement with the experimentally-measured fracture energy.

In the present work, peel tests will be performed using specimens which consist of a polyester backing-membrane supporting an acrylic pressure-sensitive adhesive adhered to a polyethylene substrate. The adhesive layer will not be ignored in the FE modelling studies because it is geometrically significant relative to the thickness of the peel arm, unlike in the model developed by Wei and Hutchinson [25]. The pressure sensitive adhesive will not be modelled as a simple linear elastic or elastic–plastic material, as done by Williams and Kauzlarich [26,27], but instead be accurately simulated as a viscoelastic material. By doing this, there is no need to develop a method for predetermining the equivalent strain rate at which to test the bulk PSA. In addition, as the strain rate is non-uniform around the peel front, it is essential that a viscoelastic model be used to represent the behaviour of the PSA. Also, in the present work the properties of the PSA-polyethylene substrate interface (which is the observed failure path from the experimental studies) will be simulated via a CZM. The cohesive zone parameters for the CZM will either (a) be directly measured experimentally from a poker-chip probe tack test, or (b) calculated from peel tests via an analytical elastic–plastic fracture mechanics approach [28]. This differs from the work of Cui et al. [23] and Martiny et al. [24] where the failure criteria were determined numerically using an inverse analysis. Further, the present FE model simulates the entire peeling process from the free peel arm bending to the initial debonding upon the start of steady-state crack propagation, whereas the FE model of Williams and Kauzlarich [26,27] did not produce debonding and that of Martiny et al. [24] modelled only the steady-state peel force.

The outline of the present paper is as follows: first the peeling process is analysed using an elastic–plastic fracture mechanics approach from which the cohesive zone parameters needed in the CZM of the PSA-substrate interface may be deduced. This is followed by a description of the visco-hyperelastic and plastic power-law material models used to define the PSA and polyester backing membrane, respectively. The mechanical characterisation methods and results used to calibrate the material models are next given for the polyester backing membrane and the PSA. The poker-chip probe tack test method is then described which gives experimental values of the tack energy and peak stress for different contact times and dwell forces. Thus, this tack test gives a second, independent and direct, source of the parameters needed for the CZM. The experimental rig and test method used for the peel experiments are described and the measured steady-state peel forces are used to calculate the fracture energy and peak stress, also for use in the CZM, via the analytical approach. Next the FE model, with an embedded CZM, is developed to simulate the peel test. The cohesive zone parameters determined from the two different methods are now used in the CZM. The numerical predictions for the peel force are compared with the experimentally measured values.

2. Analytical modelling

2.1. Peeling model

A common method of characterising the performance of a PSA adhered to a substrate is the 'simple' peel test, as shown in

Fig. 1. Kinloch et al. [28] developed an analytical peeling model based on an energy balance and large displacement beam theory in order to calculate the fracture energy, G_a, which was then implemented by Georgiou et al. [29] into an algorithm known as 'ICPeel'. The peel arm undergoes a complex bending and unbending process, during which plastic energy is dissipated. The fracture energy is determined using an energy balance:

$$G_a = \frac{1}{b}\left(\frac{dU_{ext}}{da} - \frac{dU_s}{da} - \frac{dU_t}{da} - \frac{dU_p}{da}\right) \tag{1}$$

where the terms are incremental and dU_{ext} is the external work, dU_s is the stored tensile strain energy in the peeling arm, dU_t is the energy dissipated during tensile deformation of the peeling arm and dU_p is the energy dissipated during plastic bending of the peeling arm near the peel front. Eq. (1) can be shown to lead to:

$$G_a = \frac{P}{b}(1 + \varepsilon_a - \cos\theta) - h\int_0^{\varepsilon_a} \sigma.d\varepsilon - G_p \tag{2}$$

where P is the steady-state peel force, b is the width of the specimen, θ is the peel angle, h is the thickness of the peel arm and ε_a is the tensile strain in the peeling arm. Therefore, the value of G_p needs to be determined in order to find G_a.

Alternatively, the total energy input, G, can be represented by Eq. (3) which can be split into three terms: the fracture energy, G_a, the plastic work done in bending of the peel arm, G_p, and an elastic energy release rate due to tensile stretching in the peel arm. Of note is the fact that if elastic conditions are maintained, then G_p is zero and σ_y becomes the actual stress, σ, in the peel arm. Thus, Eq. (3) becomes the same as that derived by Kendall [14]:

$$G = \frac{P}{b}(1 - \cos\theta) = G_a + G_p - \frac{\sigma_y^2 h}{2E} \tag{3}$$

The plastic work is expressed in terms of both the peel angle, θ, and the root rotation angle, θ_0, as shown in Fig. 1:

$$G_p = \frac{P}{b}[1 - \cos(\theta - \theta_0)] \tag{4}$$

During the peeling process, the bending moment, M, tends towards a plastic limit, M_p. The total energy can therefore be estimated as follows:

$$G \approx 2\frac{M_p}{b}\frac{1}{R_0} = \frac{\sigma_y h^2}{2R_0} \tag{5}$$

where σ_y is the yield stress of the peel arm and R_0 is the local radius of curvature at the peel front at the plastic limit as shown in Fig. 1.

By substituting Eq. (4) and (5) into Eq. (3), and using $\Delta = \theta_0 \cdot R_0$, where Δ is a characteristic length of deformation, an approximate expression for G_a can be obtained:

$$G_a = \left(\frac{\Delta}{h}\right)\cdot\frac{2G^2}{\sigma_y h} + \frac{\sigma_y^2 h}{2E} \tag{6}$$

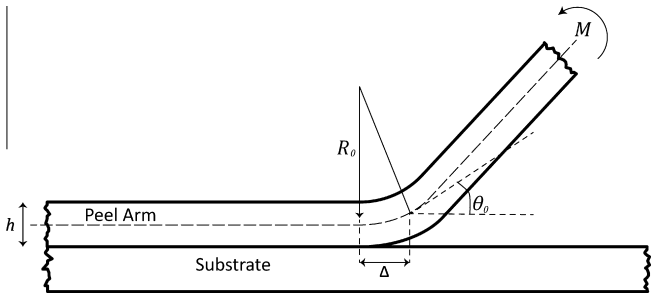


Fig. 1. Schematic of the local bending and root rotation at the peel front.

The solution for Δ comes from a beam on a linear-elastic foundation analysis and leads to a stress-displacement relationship for a CZM [29]. Therefore:

$$\left(\frac{\Delta}{h}\right)^4 = \frac{E}{3h}\left(\frac{b}{k_s}\right) \tag{7}$$

The equation above can be further expanded in terms of the elastic moduli of the peel arm, E, and the adhesive, E_a,:

$$\left(\frac{\Delta}{h}\right)^4 = \frac{1}{6}\left(1 + \frac{2h_a E}{hE_a}\right) \tag{8}$$

By substituting Eq. (8) into Eq. (6), the fracture energy, G_a, is then calculated. Since the traction-separation law takes the shape of a triangle, where the area is equal to G_a, it is thus possible to calculate the critical stress, σ_{max}. This is expressed as:

$$\sigma_{max} = 2\sqrt{\frac{\frac{G_a E}{h}}{1 + \frac{2h_a E}{hE_a}}} \tag{9}$$

In the present work, the steady-state peel force, in addition to the material parameters and dimensions of the polyester backing membrane and the PSA, are used to calculate the fracture energy and the critical stress, for later use in the CZM, via the above analytical model. It should be noted that since the PSAs are viscoelastic materials, thus rate and temperature dependent, the fracture energy is also dependent on these parameters but the analytical model described above does not account for this.

2.2. Visco-hyperelastic material model

The PSA is a non-linear viscoelastic material, hence its constitutive response under step strain relaxation is both strain- and time-dependent as described in Eq. (10) [30]. The strain-dependent function, $\sigma_0(\varepsilon)$, has the dimensions of stress while the time-dependent function, $g(t)$, is dimensionless.

$$\sigma(\varepsilon, t) = \sigma_0(\varepsilon)g(t) \tag{10}$$

where σ is the true stress at a true strain, ε, and time, t. The strain-dependent function can be non-linearly elastic through a hyperelastic potential. It should be noted that Eq. (10) assumes that the strain and time effects on the stress response are separable. In this work, the Van der Waals hyperelastic potential (Eq. (11)) is used which has the following material parameters: an instantaneous shear modulus, ψ, locking stretch constant, λ_m, and the global interaction parameter, a [31,32].

$$U_{VDW} = -\psi\left\{(\lambda_m^2 - 3)\left[\ln\left(1 - \sqrt{\frac{I_1 - 3}{\lambda_m^2 - 3}}\right) + \sqrt{\frac{I_1 - 3}{\lambda_m^2 - 3}}\right] + \frac{2}{3}a\left(\frac{I_1 - 3}{2}\right)^{\frac{3}{2}}\right\} \tag{11}$$

The true stress as a function of the stretch ratio in the direction of the load, λ, for uniaxial loading can be derived from:

$$\sigma_0 = \lambda\frac{dU_{VDW}}{d\lambda} \tag{12}$$

where for uniaxial deformation under constant volume assumptions, the stretch ratios in the principal directions are:

$$\lambda_1 = \lambda, \quad \lambda_2 = \lambda_3 = \frac{1}{\sqrt{\lambda}}$$

The time-dependent function is represented by the Prony series:

$$g(t) = g_\infty + \sum_{i=1}^{N} g_i e^{(-t/\tau_i)} \tag{13}$$

where g_∞ and g_i are dimensionless constants, τ_i are the relaxation times and $g_\infty + \Sigma g_i = 1$. Therefore, $\sigma_0(\varepsilon)$ represents the instantaneous stress–strain relationship, corresponding to $t = 0$, while $g_\infty\sigma_0(\varepsilon)$ is the long-term stress–strain relationship corresponding to $t = \infty$.

The stress, for any strain history, can be expressed using the Leaderman form of the convolution integral [33]:

$$\sigma(\varepsilon, t) = \int_0^t g(t-s)\frac{d\sigma_0(\varepsilon)}{ds}.ds \tag{14}$$

which can then be split into a long term elastic and a viscoelastic contribution, resulting in an expression for stress which is expressed solely in terms of t as shown in Eq. (15).

$$\sigma(t) = g_\infty\sigma_0(t) + \sum_{i=1}^{N}\int_0^t g_i e^{\left(-\frac{t-s}{\tau_i}\right)}\frac{d\sigma_0(s)}{ds}.ds \tag{15}$$

Since the convolution integral does not have a closed form, the integral can be solved using an algorithm based on finite increments of time. This recursive equation is shown below:

$$\sigma(t_{n+1}) = g_\infty\sigma_0(t_{n+1}) + \sum_{i=1}^{N}\left(e^{\left(-\frac{\Delta t}{\tau_i}\right)}h_i(t_n) + g_i\frac{1-e^{\left(-\frac{\Delta t}{\tau_i}\right)}}{\frac{\Delta t}{\tau_i}}[\sigma_0(t_{n+1}) - \sigma_0(t_n)]\right) \tag{16}$$

where:

$$h_i(t_n) = \int_0^{t_n} g_i e^{\left(-\frac{t_n-s}{\tau_i}\right)}\frac{d\sigma_0(s)}{ds}.ds \tag{17}$$

Eq. (16) can therefore be used to calculate the stress at any time, t_{n+1}, provided the stress at the previous time step, t_n, is known. The initial state is usually $\sigma = \varepsilon = t = 0$, hence the stress at $t > 0$ can be calculated. Eq. (16) can then be used to fit experimental stress–strain data which was measured at known time intervals. A more detailed description can be found in the work published by Goh et al. [30].

2.3. Power-law hardening material model

The polyester backing membrane is modelled using a simple power-law, as stated in Eq. (18). This model allows both the initial linear-elastic region and the plastic work-hardening region of the stress–strain curve to be expressed analytically through:

$$\sigma = \begin{cases} E\varepsilon & (\varepsilon \leqslant \varepsilon_y) \\ \sigma_y\left(\frac{\varepsilon}{\varepsilon_y}\right)^n & (\varepsilon > \varepsilon_y) \end{cases} \tag{18}$$

where is the ε_y yield strain and n is the power-law constant.

3. Experimental

All experiments were performed using a Zwick mechanical testing machine under environmental conditions of 21 °C and 50% humidity. These experiments included tensile tests, relaxation tests, probe tack tests and peeling tests.

3.1. Tensile tests of the backing membrane

The backing membrane used was a polyester film with a thickness of 20 μm which was purchased from 3M. Four film strips with a gauge length of 130 mm and width of 10 mm were tested in tension at speeds of 10, 100 and 1000 mm/min. The stress–strain curves shown in Fig. 2, were modelled using the simple power-law in Eq. (18). The elastic modulus, E, and yield stress, σ_y, were 4.44 GPa and 70 MPa respectively, while the power-law constant, n, was calculated to be 0.287. There was a small rate dependency in the plastic region which was ignored in the present study.

3.2. Tensile and relaxation tests of the PSA

An acrylic PSA, supplied by Henkel, was dissolved in a solvent and then cast between two fluoropolymer-coated release liners purchased from 3M. The solvent was subsequently allowed to evaporate fully to produce a solid acrylic polymer sheet with a thickness of 0.5 mm. PSA samples with dimensions of 50 mm × 10 mm were prepared and tested in tension at true strain rates of 0.1, 1 and 10 min^{-1} and in relaxation from elongation strains of 0.1 and 1 with an initial loading rate of 1 min^{-1}. Each test was conducted with three replicate samples. The resulting stress–strain and stress-time responses for the tensile and relaxation tests, respectively, are shown in Fig. 3. The values of the true stress and true strain were calculated using Eqs. (19) and (20):

$$\varepsilon = ln\left(1 + \frac{\Delta l}{l}\right) \tag{19}$$

$$\sigma = \frac{F}{A}\left(1 + \frac{\Delta l}{l}\right) \tag{20}$$

where l is the original length of the sample, A is the cross-sectional area of the sample and F is the force applied.

Isometric curves were plotted in Fig. 4 using the tensile data. Parallel lines were obtained for all the strains which implied that the strain- and time- dependent behaviour are separable. This justifies the use of the separable assumption made in the previous section.

The viscoelastic material model described earlier was calibrated using the data shown in Fig. 2. An optimisation algorithm, based on minimising the least square of errors [30] was used to calculate the material constants and Prony series parameters which are necessary inputs for the FE model. The Van der Waals hyperelastic potential material constants were determined as: $\psi = 0.411$ MPa, $\lambda_m = 8.56$ and $a = 0.361$. The Prony series parameters are summarised in Table 1 where the subscripts represent the time constants; these were set to range from 0.1 to 1000 s and spaced such that they were an order of magnitude apart.

3.3. Probe tack tests

Initially, standard probe tack tests were performed with a flat steel probe making contact with a significantly larger sheet of the PSA bonded to a polyethylene substrate. The basic idea was that

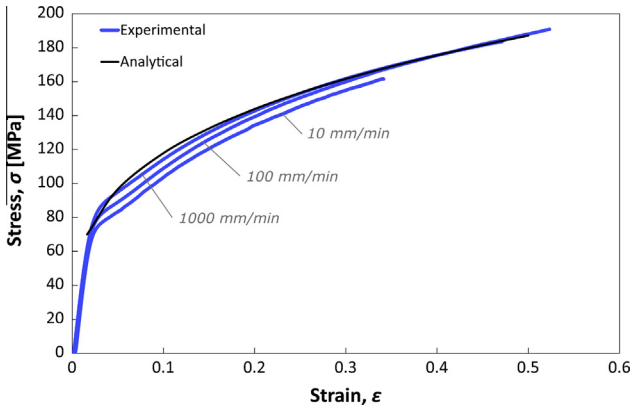


Fig. 2. The tensile stress–strain curves of the polyester backing membrane film tested at speeds of 10, 100 and 1000 mm/min and the power law analytical fit.

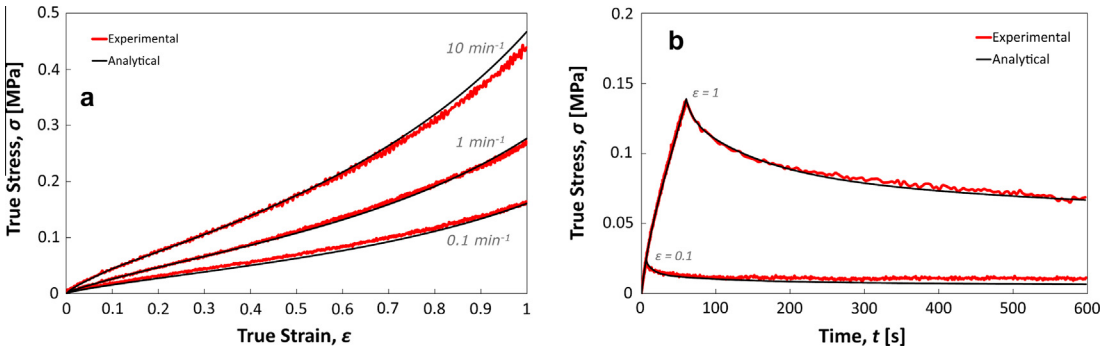


Fig. 3. (a) Tensile stress versus strain and (b) relaxation stress versus time curves of the PSA and their respective visco-hyperelastic model fits.

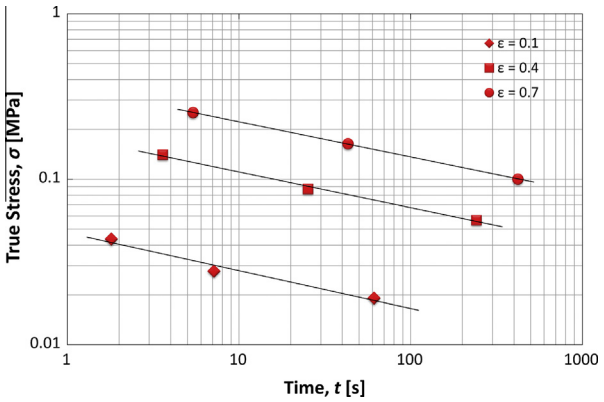


Fig. 4. Isometric plot for the PSA.

Table 1
The Prony series parameters.

Van der Waals	$g_{0.1}$	g_1	g_{10}	g_{100}	g_{1000}
	0.740	0.044	0.099	0.046	0.038

the dwell time, dwell force and pull-off speed would be varied and, the maximum stress and the tack work of adhesion could be measured and then employed in the CZM. However, all such experiments produced fibrillation of the PSA and eventual cohesive failure of the PSA itself. Since interfacial failure between the PSA and the polyethylene substrate was observed in the peel tests (to be described in the following section), the cohesive parameters from these probe tack tests were considered to be invalid. Thus, the standard probe tack test was redesigned.

A new design of 'poker-chip' probe tack test was therefore developed as a means of obtaining the cohesive parameters σ_{max} and W_a for use later in the CZM. This test method was similar to that used by Cooper et al. [34] in which circumferentially deep-notch tensile (CDNT) specimens were used to directly measure the cohesive zone parameters. PSA films of 13 mm diameter and 150 μm thickness were applied to a sheet of the polyethylene substrate and then a 15.6 mm diameter steel probe was brought into contact with the PSA surface. Upon pulling-off the steel probe and the attached PSA, there was no observable fibrillation of the PSA and, as expected, failure occurred at the PSA-polyethylene interface instead of cohesively.

Typical force–time and stress-displacement curves from the poker-chip probe tack test are shown in Fig. 5. The tack work of adhesion, W_a, taken to be equivalent to G_a for use in the CZM, was calculated from the area under the positive section of the stress-displacement graph while the tack strength, σ_{max}, was measured directly as the peak stress on the same graph.

Each time the dwell force or dwell time was varied, at least six replicate experiments were conducted. The dwell force was varied in the range of 1–20 N with a pull-off speed of 10 mm/min and a dwell time of 200 s. The resulting values of W_a and σ_{max} are plotted as a function of the dwell force in Fig. 6.

Even though the experimental scatter shown in Fig. 6 is rather large, it was concluded that above a dwell force of about 1 N there was no significant effect on either W_a and σ_{max}. Thus, for future probe tack tests the dwell force was kept at 10 N. Next, the dwell time was varied between 10 and 300 s and the probe was pulled-off at a speed of 100 mm/min. As before, a minimum of six replicate samples were tested for each dwell time. Despite the scatter, the dwell time had no statistical effect on the results, as shown in Fig. 7. The results presented here are consistent with those of Creton and Leibler [12], which showed that for a smooth surface, the maximum tack stress was independent of dwell force and time above a minimum value. Nakamura et al. [11] showed that there was a very gradual rise in the tack work of adhesion as the dwell time was increased.

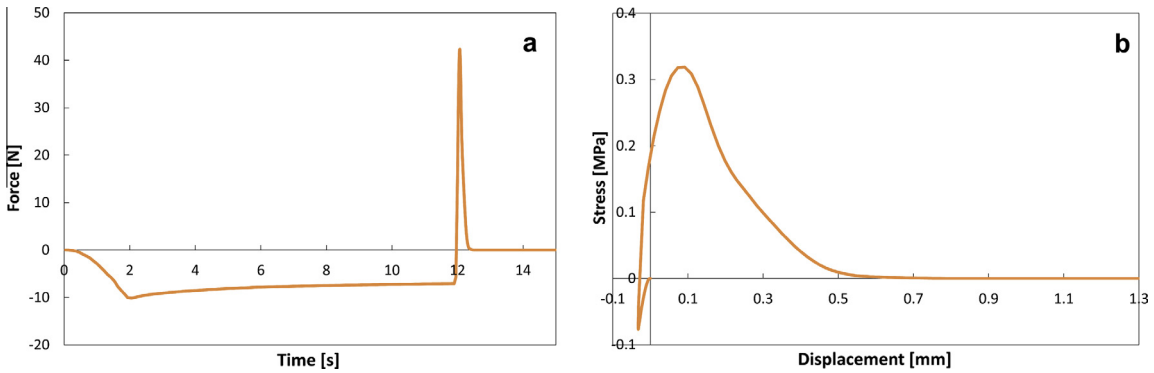


Fig. 5. (a) Tack force versus time and (b) tack stress versus displacement for a dwell force of 10 N, dwell time of 10 s and pull-off speed of 100 mm/min.

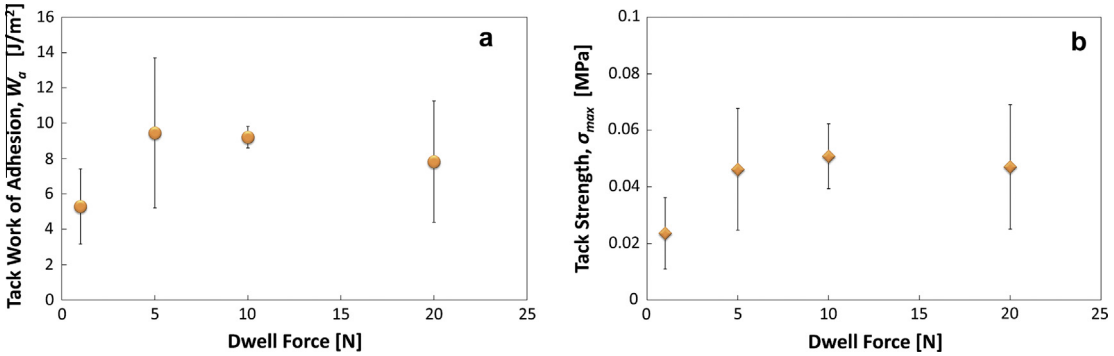


Fig. 6. (a) The tack work of adhesion, W_a, and (b) tack strength, σ_{max}, at different dwell forces for a dwell time of 200 s and pull-off speed of 10 mm/min.

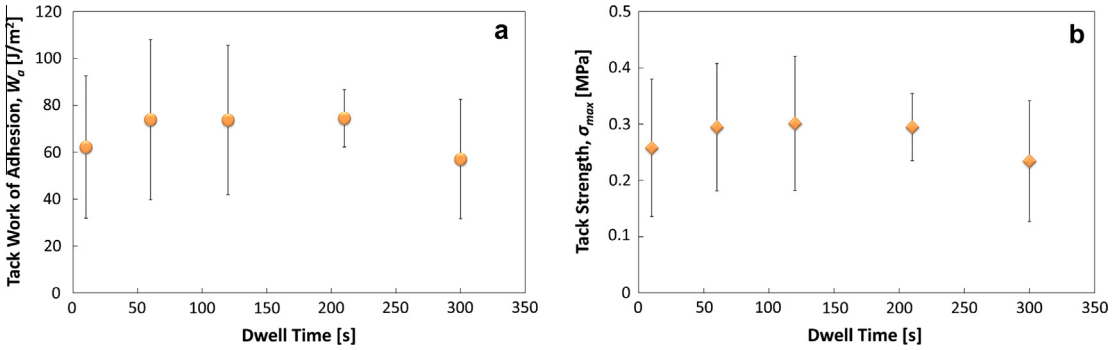


Fig. 7. (a) The tack work of adhesion W_a, and (b) tack strength, σ_{max}, at different dwell times for a dwell force of 10 N and pull-off speed of 100 mm/min.

Therefore at 100 mm/min the tack work of adhesion, W_a, (=G_a) and the tack strength, σ_{max}, obtained were 70 J/m^2 and 0.3 MPa respectively. Since the peel tests were also undertaken at a rate of 100 mm/min, these values will be employed later in the FE simulations of the peel tests.

3.4. Peel Tests

Peel test specimens were prepared by casting the acrylic PSA onto the polyester backing membrane to give an adhesive thickness of 150 μm. It should be noted that this value of the PSA thickness was the same as that used for the probe tack tests, see Section 3.2. After the solvent had fully evaporated, the release liner was placed on the PSA to protect its bonding surface and the assembled tape was then cut into 20 mm wide and 80 mm long strips ready to be used for the peel tests. The release liner was removed from the surface of the PSA and approximately 40 mm of the tape length was then applied to the polyethylene substrate using a roller which ensured that a high enough dwell force was achieved to produce complete bonding. The free-end of the peel arm was fixed to a tensile grip on the mechanical testing machine. The polyethylene substrate was attached to a 80 mm × 40 mm IKO precision linear slide with a stroke length of 47 mm, which ensured that a constant peel angle was maintained during the test. Peel tests were performed at a constant peel crack speed of 100 mm/min and peel angles of 45°, 90°and 135°. At each angle, the peel test was repeated three times. For the 45° and 135° experiments, the polyethylene substrate sheet was attached to a triangular block, which in turn was attached to the trolley, as shown in Fig. 8.

The crack speed, $\dot{a}$, was maintained constant for each peel angle, θ, by adjusting the crosshead speed, $\dot{x}$, according to Eq. (21) [16]:

$$\dot{x} = \dot{a}(1 - \cos\theta) \tag{21}$$

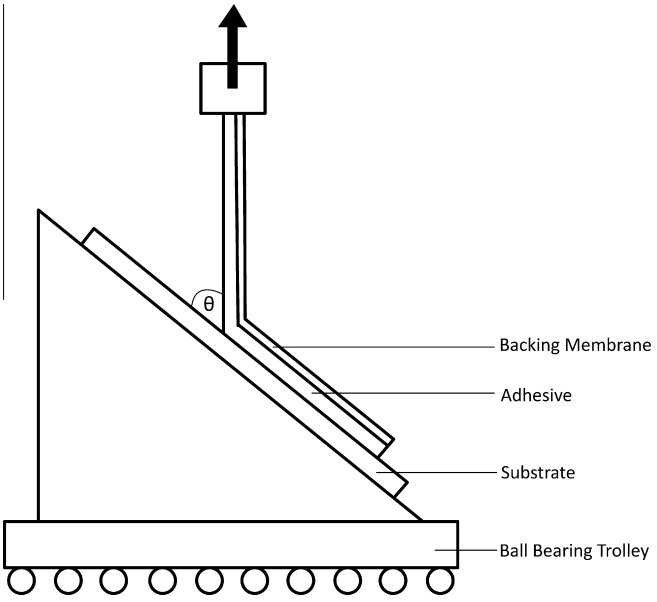


Fig. 8. A schematic of the experimental peel rig.

Interfacial failure occurred between the PSA and the polyethylene substrate without fibrillation of the PSA. The recorded steady-state peel force decreased as the peel angle increased, as shown in Table 2.

The geometry and material properties of the peel arm and the parameters required to calculate the fracture energy using the analytical model [28,29] are given in Section 2. The PSA modulus, E_a, was estimated by multiplying the instantaneous shear modulus, ψ, obtained from the viscoelastic material model, by a factor of

Table 2
The peel force, fracture energy, maximum stress and plastic-energy dissipated for each peel angle.

Peel angle, θ (°)	Peel force, P (N)	Fracture energy, G_a (J/m^2)	Maximum stress, σ_{max} (MPa)	Plastic energy, G_p (J/m^2)
45	5.89 ± 0.61	83.9 ± 8.8	1.17 ± 0.06	2.8 ± 0.2
90	2.19 ± 0.21	94.1 ± 9.4	1.24 ± 0.06	15.3 ± 1.0
135	1.79 ± 0.13	115.7 ± 9.1	1.38 ± 0.05	37.0 ± 1.6

three. It should be noted that, in the present analytical modelling studies, the peel arm was taken to consist of only the polyester backing membrane. Further, since the very low modulus PSA had little influence on the properties of a combined peel arm of the polyester backing membrane together with the PSA, this simplification affected the values of G_a and σ_{max} by no more than 10%, 3% and 0.5% for the peel angles of 135°, 90° and 45° respectively.

The values of the fracture energy, G_a, and the maximum stress, σ_{max}, so calculated at each angle are shown in Table 2. It is observed that there was an increasing trend in G_a and σ_{max} with θ, but this is not statistically significant with an average value of 98 J/m^2 and 1.26 MPa, respectively. Also of note is that the value of G_p is considerably smaller than G_a but also shows a tendency to increase in value as the peel angle increases.

4. Numerical modelling of peeling

4.1. Introduction

A two-dimensional, plane strain simulation of the peel test was performed using the commercial FE software Abaqus [35]. The entire assembly consisted of two parts: an analytical rigid-body representing the polyethylene substrate and a 2D deformable body for the peel arm, which was then partitioned into the polyester backing membrane and the PSA adhesive components. (Thus, unlike the above analytical model, the FE simulations can readily model the peel arm as consisting of two materials, see Fig. 9). The polyester backing membrane and the PSA were modelled using the elastic–plastic and visco-hyperelastic material models described in Section 2 above. A CZM was implemented at the interface between the PSA and the polyethylene substrate, to simulate interfacial failure, as was indeed observed experimentally. The free end of the peel arm was displaced in the required loading direction, while the rigid polyethylene substrate was restrained both horizontally and vertically. A schematic of the FE model is shown in Fig. 9.

In the present work, cohesive contact was used instead of cohesive elements. Previous peeling simulations, not presented here, showed that for a given traction-separation law, both methods gave identical results. However, cohesive contact was an easier and a more logical approach to implement because failure via peel crack growth occurred at the interface between the PSA and the polyethylene substrate.

A mesh sensitivity analysis, using linear elements, was performed in order to determine the optimal level of mesh refinement which was computationally efficient without compromising the accuracy of the results. This was found to be two and three elements thick for the backing membrane and the PSA, respectively, with an element length of 50 μm. This mesh density was used in all future models.

4.2. Mixed-mode considerations

The mixed-mode behaviour was assumed to be mode-independent, i.e. the fracture energy was the same for both Mode I (normal) and Mode II (shear) failure. Thus, it was assumed that that $G_{Ic} = G_{IIc} = G_a$. Similarly, the normal peak stress, σ_{max}, was assumed

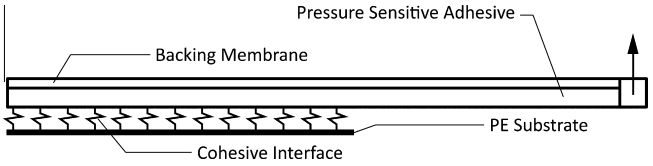


Fig. 9. The CZM/FE model and its boundary conditions (not to scale).

to be equal to the shear peak stress. Thus, the Mode I and Mode II traction-separation laws were taken to be identical, since the same initial stiffness, k, was also specified. Damage was initiated based on a maximum stress criterion, σ_{max}, in both the normal and shear loading modes followed by a linear progressive damage evolution. The mixed-mode failure locus for G_{Ic} and G_{IIc} was linear and defined by:

$$\frac{G_I}{G_{Ic}} + \frac{G_{II}}{G_{IIc}} = 1 \tag{22}$$

The implications of the above assumptions are discussed in detail below.

4.3. The traction-separation law

A triangular traction-separation law was employed with the two parameters σ_{max} and G_a defining the CZM. However, a third parameter was also required, namely the initial stiffness, k. A parametric study was performed to determine the influence of k on the predicted peel force, with σ_{max} and G_a set to 0.3 MPa and 70 J/m^2, respectively. The latter are the values obtained from the poker-chip probe tack tests, shown in Fig. 7, which were performed at the same rate of 100 mm/min as that used for the peel tests. The results from this parametric study shown in Fig. 10 reveal that there is a threshold value beyond which the predicted peel force remained constant. A relatively large value for k did not introduce artificial compliance in the model, and therefore for all future simulations the value of k was set equal to 5×10^{11} Pa/m.

4.4. Numerical predictions

As discussed above, the σ_{max} and G_a values for the CZM were obtained using two different test methods: (a) calculated values from using the analytical model of the peel test (i.e. 1.26 MPa and 98 J/m^2), and (b) direct experimental measurements from the poker-chip probe tack test (i.e. 0.3 MPa and 70 J/m^2 (where $G_a = W_a$)). As may be seen from these results, the values of G_a from the two different test methods are not very different but the values of σ_{max} differ considerably. Nevertheless, as discussed above, it had been decided to implement both pairs of values in the CZM, since an aim of the present work was to attempt to derive the values for the CZM from analytical or independent experimental studies.

The simulation of the peel tests that used the analytically calculated CZM parameters of 1.26 MPa and 98 J/m^2 exhibited no debonding because the nodes at the PSA-polyethylene interface never attained the prescribed critical stress. Instead, the model predicted that the peel arm would simply continue to undergo tensile stretching and no peel crack growth would ever occur.

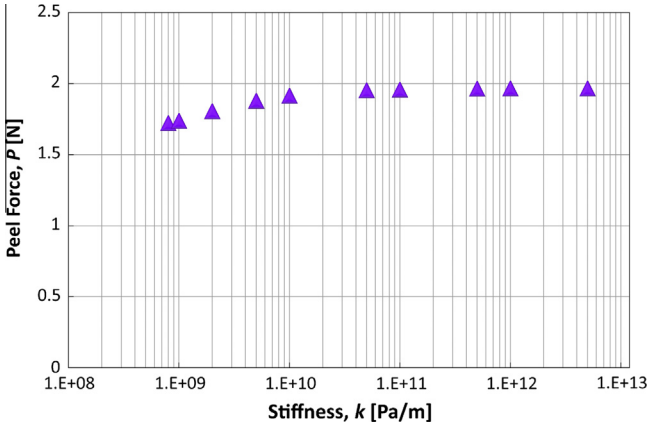


Fig. 10. The influence of the cohesive stiffness on the predicted peel force at 90°.

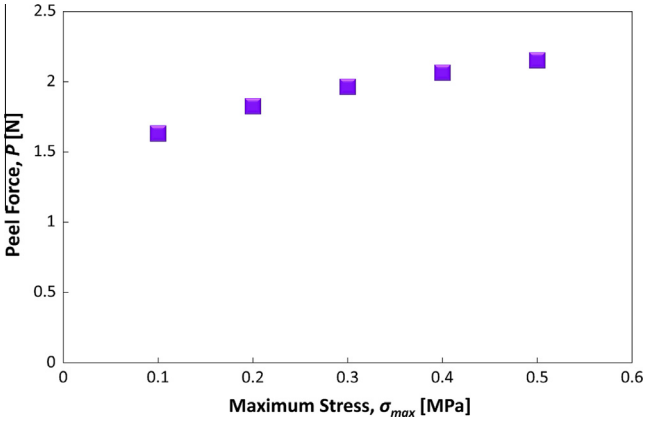


Fig. 12. The influence of the maximum stress on the predicted peel force at 90° as obtained from the numerical model using a G_a value of 70 J/m^2.

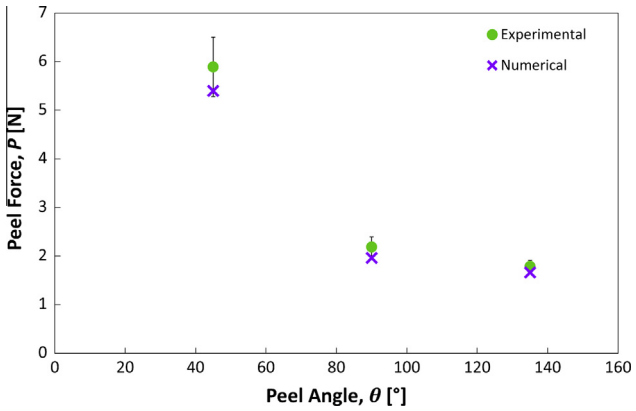


Fig. 11. The numerical and experimental peel forces for different peel angles at a crack speed of 100 mm/min. The σ_{max} and G_a values were from the probe tack test and were 0.3 MPa and 70 J/m^2, respectively.

In contrast, the simulations did predict that peel crack growth would occur when the CZM employed the probe tack values of σ_{max} and G_a of 0.3 MPa and 70 J/m^2. Further it was observed that there was a very good agreement between the numerically predicted and the experimentally-measured values of the peel force. This may be seen from Fig. 11 where the numerical and experimental peel forces, at different peel angles, are compared. These results demonstrated the validity of using the probe tack test to obtain σ_{max} and G_a.

4.5. Parametric study of the effect of σ_{max}

Since the numerical model failed to converge using the analytically calculated CZM parameters, a parametric analysis was performed to determine the effect on the predicted peel force upon varying the value of σ_{max} in the CZM. The results in Fig. 12 show that there is an increasing trend of the peel force with σ_{max}. Above a certain value of σ_{max} (i.e. 0.5 MPa) the crack would not propagate, instead the free end of the peel arm simply undergoes tensile deformation, and the model would abort. Diehl [22], who performed peeling simulations with an Abaqus Explicit solver over three orders of magnitude of σ_{max} values, also reported that there was a value above which his CZM/FE model performed poorly.

The present results in Fig. 12 show that not only the value of G_a is important to obtain an accurate CZM/FE simulation but that the value of σ_{max} also has a major influence on the predicted peel force. This observation agrees with the work of Blackman et al. [17] who emphasised that the outcome of the CZM was typically dependent upon the values of both of these CZM parameters. Indeed, Tantideeravit et al. [32] have also shown that there was in increase in the predicted peel force as the value of σ_{max} was increased. This is in contrast to Diehl's use of a single-parameter cohesive law, dependent only on G_a, which relied upon the extrapolation of a mesh-relative factor in order to obtain a numerical peel strength value [22].

Therefore, it may be concluded that the analytical model of the peel test, which led to a σ_{max} value of 1.26 MPa, resulted in a value which is excessively high. This observation can also be deduced by a comparison with the tensile test data of the PSA, see Fig. 3, where the true stress values are far less than 1.26 MPa. Since the value of σ_{max} from the peel test was clearly too high, an inverse analysis was performed by reducing σ_{max} but keeping G_a to be 98 J/m^2 (as calculated from the analytical model of the peel test), until the peel force predicted from the numerical CZM/FE simulations agreed with the experimentally-measured peel force. The value of σ_{max} that was needed for such an agreement was found from this inverse analysis to be 0.12 MPa, which is very close to the measured value obtained from the poker-chip probe tack tests.

4.6. Effect of mode-mix

As already mentioned above, it was assumed that G_{Ic} was equal to G_{IIc}, and hence to G_a, and the value of σ_{max} was also kept constant irrespective of whether Mode I or Mode II loading was being considered. These assumptions are justified theoretically since such peel tests are considered to be under predominantly Mode I loading conditions [24,25,28]. In order to further confirm the validity of these assumptions, the mode-mix was verified using the numerical model. The individual traction-separation data were plotted using the normal and shear stresses and their respective displacements of any node in the cohesive zone at steady state for each peel angle, as shown in Fig. 13.

By dividing the area under the Mode I and Mode II lines, the mixed-mode ratio for each peel angle was determined, as shown in Fig. 14. Using this method, the contribution due to Mode II (shear) was less than 5% for each peel angle. Hence, the assumption that the peeling process is mainly Mode I is indeed justified. It should also be noted that the numerical G_I and G_{II} values satisfy Eq. (22).

In addition, another simulation was performed as in Tantideeravit et al. [32], where the G_{IIc} value was set to be twice that of the G_{Ic} value, i.e. 140 J/m^2, in the 90° peeling simulation. This resulted in a peel force less than 3% higher than the peel force obtained when G_{Ic} and G_{IIc} were equal. This result further justifies the dominance of Mode I failure in the present peel tests.

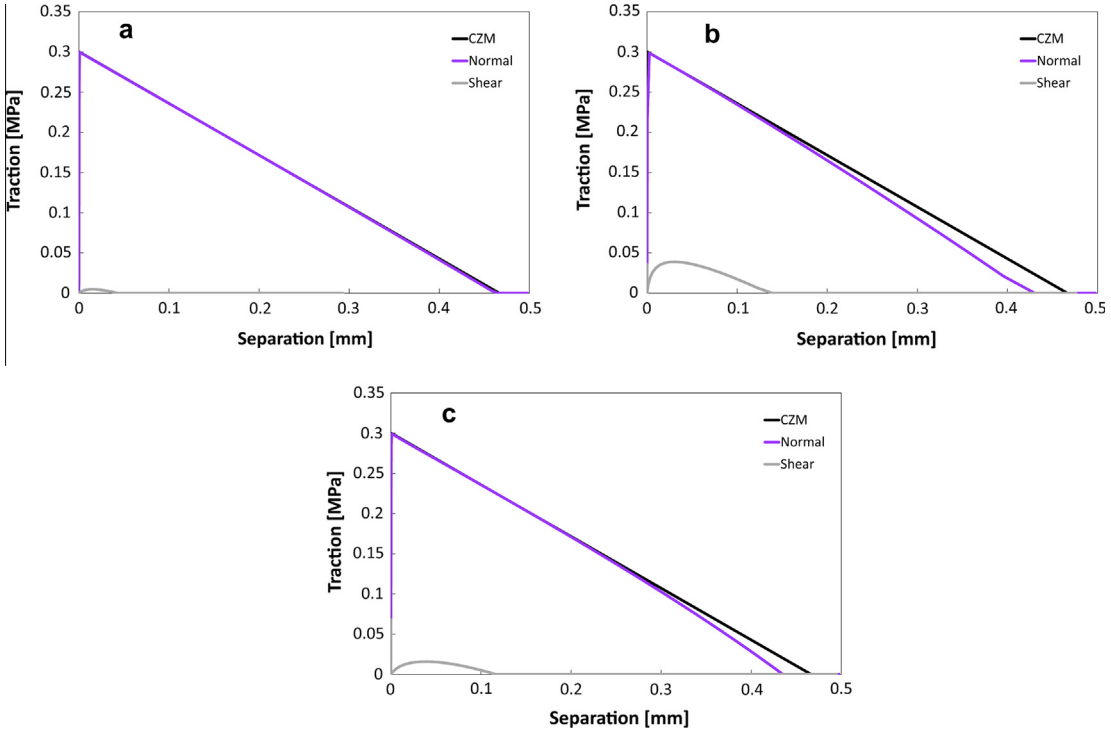


Fig. 13. Individual normal and shear traction-separation laws for (a) 45°, (b) 90° and (c) 135° peel angles.

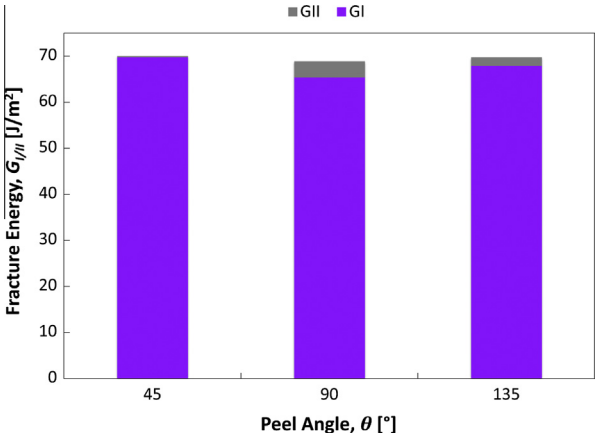


Fig. 14. The predicted mixed-mode distribution for different peel angles at a crack speed of 100 mm/min.

5. Conclusions

Fixed arm peel tests have been performed using specimens which consisted of a polyester backing membrane supporting an acrylic pressure-sensitive adhesive (PSA) adhered to a polyethylene substrate. The tests were undertaken at various peel angles, at a constant rate of crack growth, and the peel forces needed to cause crack growth along the PSA-polyethylene substrate interface were measured.

Finite element (FE) peeling simulations were conducted which modelled the backing membrane as an elasto-plastic power-law material and the adhesive as a visco-hyperelastic material. The material properties of the polyester backing membrane and the PSA were measured from tensile and stress-relaxation experiments. The properties of the PSA-polyethylene substrate interface were modelled using a cohesive zone model (CZM). The parameters required for the CZM, namely the critical stress, σ_{max}, and the fracture energy, G_a, were calculated analytically from the peel test, as well as being measured directly from an independent 'poker-chip' probe tack test. The latter method was found to give the more meaningful values of the CZM parameters. Thus, the values of σ_{max} and G_a from the poker-chip probe tack test, measured at the appropriate rate of test, were used to undertake predictions of the behaviour of the peel tests using the FE model.

It was found that the numerically predicted peel forces were in good agreement with the experimentally measured peel forces over the range of peel angles studied. The accuracy of the FE peeling model supported the poker-chip probe tack method for determining independently, by direct measurement, the CZM parameters of σ_{max} and G_a. Further validation of the model is needed and current work is focussing on testing its accuracy for various peel rates and PSA thicknesses.

Acknowledgements

The authors would wish to thank the EPSRC, UK for financial support and Henkel for supplying the pressure-sensitive adhesive. We also wish to express our thanks to Dr. Sudax Murdan and Dr. Khalida Rizi from the UCL School of Pharmacy for their advice with specimen preparation. Special thanks are due to Prof. J. Gordon Williams for his helpful and insightful discussions on the peel test and the analytical peel model.

References

[1] C. Creton, Pressure-sensitive adhesives: an introductory course, MRS Bull. 28 (2003) 434–439.
[2] B. Zhao, R. Pelton, Peel adhesion to paper—interpreting peel curves, J. Adhes. Sci. Technol. 17 (2003) 815–830.
[3] B. Zhao, L. Anderson, A. Banks, R. Pelton, Paper properties affecting pressure-sensitive tape adhesion, J. Adhes. Sci. Technol. 18 (2004) 1625–1641.
[4] S. Venkatraman, R. Gale, Skin adhesives and skin adhesion: 1. Transdermal drug delivery systems, Biomaterials 19 (1998) 1119–1136.

[5] H.S. Tan, W.R. Pfister, Pressure-sensitive adhesives for transdermal drug delivery systems, Pharm. Sci. Technol. Today 2 (1999) 60–69.
[6] R.H. Plauta, Two-dimensional analysis of peeling adhesive tape from human skin, J. Adhes. 86 (2010) 1086–1110.
[7] J. Zhou, W. Yu, S.P. Ng, Methods of studying breast motion in sports bras: a review, Text. Res. J. 81 (2011) 1234–1248.
[8] W.K. Chiang, E. Ghassemieh, R. Lewis, J. Rowson, C. Thompson, Comparison of tack of pressure-sensitive Adhesives (PSAs) at different temperatures, J. Adhes. Sci. Technol. 24 (2010) 1949–1957.
[9] B. Duncan, S. Abbott, R. Roberts. Measurement Good Practice Guide No. 26: Adhesive Tack, National Physical Laboratory, Teddington, United Kingdom, 1999.
[10] Y. Nakamura, K. Imamura, K. Yamamura, S. Fujii, Y. Urahama, Influence of crosslinking and peeling rate on tack properties of polyacrylic pressure-sensitive adhesives, J. Adhes. Sci. Technol. 27 (2013) 1951–1965.
[11] Y. Nakamura, K. Imamura, K. Ito, S. Nakano, A. Sueoka, S. Fujii, M. Sasaki, Y. Urahama, Contact time and temperature dependencies of tack in polyacrylic block copolymer pressure-sensitive adhesives measured by the probe tack test, J. Adhes. Sci. Technol. 26 (2012) 231–249.
[12] C. Creton, L. Leibler, How does tack depend on time of contact and contact pressure?, J Polym. Sci., Part B: Polym. Phys. 34 (1996) 545–554.
[13] P. Tordjeman, E. Papon, J.-J. Villenave, Tack properties of pressure-sensitive adhesives, J. Polym. Sci., Part B: Polym. Phys. 38 (1999) 1201–1208.
[14] K. Kendall, Thin-film peeling-the elastic term, J. Phys. D Appl. Phys. 8 (1975) 1449.
[15] D.R. Moore, An Introduction to the Special Issue on Peel Testing, Int. J. Adhes. Adhes. 28 (2008) 153–157.
[16] D.R. Moore, J.G. Williams, A protocol for determination of the adhesive fracture toughness of flexible laminates by peel testing: fixed arm and t-peel methods, An ESIS Protocol, Imperial College London, 2010.
[17] B.R.K. Blackman, H. Hadavinia, A.J. Kinloch, J.G. Williams, The use of a cohesive zone model to study the fracture of fibre composites and adhesively-bonded joints, Int. J. Fract. 119 (2003) 25–46.
[18] J.G. Williams, H. Hadavinia, Analytical solutions for cohesive zone models, J. Mech. Phys. Solids 50 (2002) 809–825.
[19] H. Hadavinia, L. Kawashita, A.J. Kinloch, D.R. Moore, J.G. Williams, A numerical analysis of the elastic-plastic peel test, Eng. Fract. Mech. 73 (2006) 2324–2335.
[20] R.A. Sauer, Enriched contact finite elements for stable peeling computations, Int. J. Numer. Meth. Eng. 87 (2011) 593–616.
[21] D. Taylor, The theory of critical distances, Eng. Fract. Mech. 75 (2008) 1696–1705.
[22] T. Diehl, On using a penalty-based cohesive-zone finite element approach, Part II: Inelastic peeling of an epoxy-bonded aluminum strip, Int. J. Adhes. Adhes. 28 (2008) 256–265.
[23] J. Cui, R. Wang, A.N. Sinclair, J.K. Spelt, A calibrated finite element model of adhesive peeling, Int. J. Adhes. Adhes. 23 (2003) 199–206.
[24] Ph. Martiny, F. Lani, A.J. Kinloch, T. Pardoen, Numerical analysis of the energy contributions in peel tests: a steady-state multilevel finite element approach, Int. J. Adhes. Adhes. 28 (2008) 222–236.
[25] Y. Wei, J.W. Hutchinson, Interface strength, work of adhesion and plasticity in the peel test, Recent Adv. Fract. Mech. (1998) 315–333.
[26] J.A. Williams, J.J. Kauzlarich, Application of the bulk properties of an acrylic pressure-sensitive adhesive to peeling, J. Adhes. Sci. Technol. 21 (2007) 515–529.
[27] J.A. Williams, J.J. Kauzlarich, Application of the bulk properties of a silicone PSA to peeling, Int. J. Adhes. Adhes. 28 (2008) 192–198.
[28] A.J. Kinloch, C.C. Lau, J.G. Williams, The peeling of flexible laminates, Int. J. Fract. 66 (1994) 45–70.
[29] I. Georgiou, H. Hadavinia, A. Ivankovic, A.J. Kinloch, V. Tropsa, J.G. Williams, Cohesive zone models and the plastically deforming peel test, J. Adhes. 79 (2003) 239–265.
[30] S.M. Goh, M.N. Charalambides, J.G. Williams, Determination of the constitutive constants of non-linear viscoelastic materials, Mech. Time-Dependent Mater. 8 (2004) 255–268.
[31] M.A.P. Mohammed, E. Tarleton, M.N. Charalambides, J.G. Williams, Mechanical characterization and micromechanical modeling of bread dough, J. Rheol. 57 (2013) 249.
[32] S. Tantideeravit, M.N. Charalambides, D.S. Balint, C.R.T. Young, Prediction of delamination in multilayer artist paints under low amplitude fatigue loading, Eng. Fract. Mech. 112–113 (2013) 41–57.
[33] J.G.Williams. Stress Analysis of Polymers. in: 2nd ed. John Wiley & Sons, 1980.
[34] V. Cooper, A. Ivankovic, A. Karac, D. McAuliffe, N. Murphy, Effects of bond gap thickness on the fracture of nano-toughened epoxy adhesive joints, Polymer 53 (2012) 5540–5553.
[35] Abaqus Version 6.13. Hibbitt Karlsson and Sorensen Inc, Providence, USA.